Lab on a Chip

Accepted Manuscript

ROYAL SOCIETY OF CHEMISTRY

www.rsc.org/loc

Journal Name

ARTICLE

Deformation of double emulsions under conditions of flow cytometry hydrodynamic focusing

Received 00th January 20xx,
Accepted 00th January 20xx

DOI: 10.1039/x0xx00000x

www.rsc.org/

Shaohua Ma[a,b], Wilhelm T. S. Huck[a,c], Stavroula Balabani[d]†

Water-in-oil-in-water (w/o/w) microfluidics double emulsions offer a new route to compartmentalise reagents into isolated aqueous microenvironments while maintaining an aqueous carrier fluid phase; this enables compatibility with commercial flow cytometry systems such as fluorescence-activated cell sorting (FACS). Double emulsion (inner core) deformation under hydrodynamic focusing conditions that mimic the environment double emulsions experience in flow cytometry applications is of particular importance for droplet stability and cell viability. This paper reports on an experimental study of the dynamic deformation of aqueous cores of w/o/w double emulsions under hydrodynamic focusing, with the sheath flow directed at 45° to the sample flow. A number of factors affecting the inner core deformation and recovery were examined. Deformation was found to depend significantly on the core or shell viscosity, the droplet-to-sheath flow velocity ratio, and core and shell sizes. Core deformation was found to depend more on the type of surfactant rather concentration with high molecular weight surfactant exhibiting a negligible effect on deformation whereas low molecular weight surfantant enhancing deformation at low concentrations due to their lateral mobility at the interface.

Introduction

Droplet-based microfluidics has evolved into an important platform for high-throughput/high-resolution biological and chemical analysis and diagnostics, particularly at the single cell or single molecule level, by screening single objects in individual (mostly aqueous) droplets surrounded by a continuous liquid phase (mostly oil).[1-5] Double emulsions have attracted considerable attention in a range of applications such as controlled release,[6-8] materials fabrication,[9-11] cosmetics,[12] and modelling of bioreactors.[13,14] The level of deformation the droplets experience due to the hydrodynamic stresses acting on them is an important aspect of droplet-based microfluidics.

Numerous studies[15-20] have reported on the deformation and break up of single droplets in flow, dating back to the early work of Taylor;[21] however, much less research effort has been expended on the deformation of double emulsions (or compound droplets). The fluid mechanics of compound droplets is reviewed by Johnson and Sandal.[22] Compound droplets can exist in three configurations depending on the interfacial tension between the three phases (or the spreading coefficient): non-engulfing, complete engulfing and partial engulfing.[23] Experimental and numerical studies on the deformation of concentric and eccentric compound droplets that are either static or move in idealised flows have been reported in the literature.[24-26] Most recent studies on compound droplet deformation are numerical, based on boundary element methods. For example, Qu and Wang[25] applied a 3D spectral boundary element method to study dynamics of eccentric droplets in extensional flows; Hua *et al.*[26] applied the immersed boundary method to study deformation of compound droplets in shear flow and Zhou *et al.*[27] in a contracting flow. Tao *et al.* extended the boundary element method to study the deformation of double emulsions with multiple inner cores flowing through a cylindrical contracting geometry.[28] In the above compound droplet studies the inner cores were fully engulfed (concentric or eccentric) by the shell and the emphasis has been on the effect of the inner droplet on the deformation or breakup of the outer shell. In contrast, deformation of double emulsions under conditions encountered in practical applications such as sheath flow focusing in flow cytometry remains fairly unexplored. It has been reported that normal and shear stresses can cause cell injuries,[29-32] which is often a concern when fragile cell samples are processed in commercial flow cytometry such as fluorescence-activated cell sorting (FACS) as the sample stream is focused by high flow rate sheath flows. Water-in-oil (w/o) droplets are typically dispersed in oil, whereas the sheath fluid in FACS is aqueous, rendering such w/o droplets systems unsuitable for flow cytometry applications. As an alternative, water-in-oil-in-water (w/o/w) double emulsions have been shown to be (a) compatible with

[a] Department of Chemistry, University of Cambridge, Cambridge, CB2 1EW, UK
[b] Chemistry Research Laboratory, University of Oxford, Oxford, OX1 3TA, UK
[c] Radboud University Nijmegen, Institute for Molecules and Materials, Heyendaalseweg 135, 6525, AJ Nijmegen, The Netherlands
[d] Department of Mechanical Engineering, University College London, London, WC1E 7JE, UK
† Corresponding author. Email: s.balabani@ucl.ac.uk
Electronic Supplementary Information (ESI) available: videos of double emulsion deformation. See DOI: 10.1039/x0xx00000x

FACS,[33] as both the carrier fluid and the sheath fluid are aqueous, and (b) suitable candidates to compartmentalise and protect fragile cells in FACS, by reducing the shear induced stresses by nearly one-order of magnitude.[34]

Studies on hydrodynamic stress and cell damage in FACS indicate that the nozzle constriction induces highly extensional flows that potentially can damage cells[35] and hence the flow focussing point merits further investigation. According to the literature, the deformation of the aqueous cores of w/o/w double emulsions - where targeted objects are compartmentalised - in confined geometries, depends on various factors such as surface tension, viscosity ratio, capillary number (*Ca*) and the degree of confinement.[17,36-38] These factors have been studied for stationary double emulsion deformation under planar extensional flows.[24,25] In these studies, completely engulfed compound droplets are considered and the deformation is often simplified as transition from a spherical cross sectional shape to an elliptical one, which is not typically the case in double emulsions in microfluidic flows, as the inner cores are naturally deformed by the engulfing/enclosing oil shells. Unlike double emulsions moving in round capillaries adopting concentric or eccentric morphologies with the inner core in the front or middle of the shell,[39,40] double emulsions in rectangular microchannels in contact with the channel walls typically adopt an eccentric morphology as the inner core is pushed by internal circulation to the rear of the shell.[34,41]

In this work, the sheath flow focusing induced deformation of inner cores of w/o/w double emulsions is studied experimentally and compared to that of w/o simple droplets. Subsequently the factors affecting core deformation are investigated; these include surface tension, core-shell viscosity ratio, core size (*or* degree of confinement) and core-to-shell size ratio. The study can aid the design of double emulsion systems that minimize deformation due to the hydrodynamic stresses from sheath flow focusing, and provide microenvironments suitable for cell screening applications such as FACS.

Materials and Methods

All chemicals were used after purchasing from commercial suppliers without further purification. Deionised water (DIW) was used in all aqueous phases. Microfluidic PDMS devices were fabricated by combined photo- and soft-lithography,[42] described in detail previously.[43] The microchannels were fabricated by spin-coating 25 µm SU8-2025 (MicroChem, USA) onto a 3-inch silicon wafer (Compart Technology Ltd. UK), followed by pre-bake, UV exposure, and post-bake, according to the protocol from the SU8 supplier.[44] The microchannel geometry is shown in Fig 1a. The double emulsion formation channel (upstream of the sheath focusing junction) is 120 µm wide, and the straight channel downstream of the sheath focusing junction is 240 µm wide and 20 mm long. Selective surface modification was adopted to form w/o/w double emulsions, by sequentially depositing polyelectrolytes layer-by-layer and flushing silane in selected regions[41] so that the region between the first and second flow focusing junctions (A) becomes hydrophobic and the one downstream of the second flow focusing junction (B) hydrophilic. For single w/o droplets, the channel region between the first and the sheath flow focusing junctions was made hydrophobic, and downstream of the sheath flow focusing junction to the outlet hydrophilic. The entire channel was 25 µm deep, which is nearly one tenth of the channel width downstream of the sheath flow focusing junction. Hence the flow can be considered two dimensional therein. The droplet shapes (single and compound ones) were visualised in the *xy* plane at mid channel height and assumed to be ellipsoidal with a major and minor axis *a* and *b* respectively. The channel length was selected to allow double emulsions to recover fully after deformation and to avoid any flow disturbances from the outlet. The double emulsions studied typically ranged from 0.15 to 0.30 nl, and the inner core volume lies in the 0.06 – 0.20 nl range.

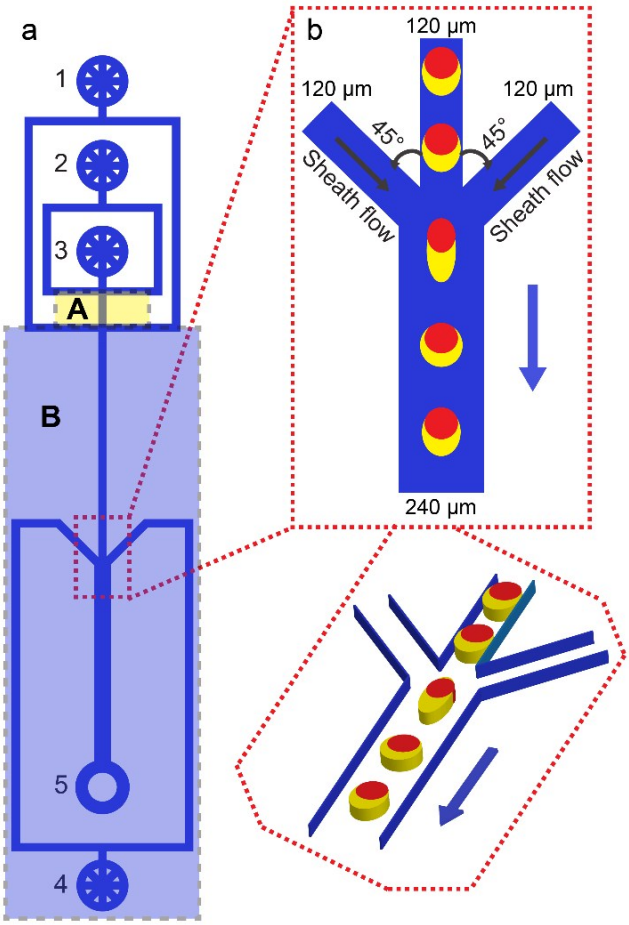

Fig 1 Double emulsion deformation setup. (a) Microfluidic channel geometry for double emulsion formation and deformation. The aqueous inner phase, oil middle phase, and aqueous outer phase are injected into the microfluidics channel via inlets 3, 2, 1, respectively; the aqueous sheath fluid is injected via inlet 4; all fluids exit via outlet 5. W/o/w double emulsions form at the second flow focusing region. (b) Zoom-in of the double emulsion (red-core-yellow-shell) deformation region under sheath flow focusing (above) and 3D view of the zoom-in region (below).

Journal Name

ARTICLE

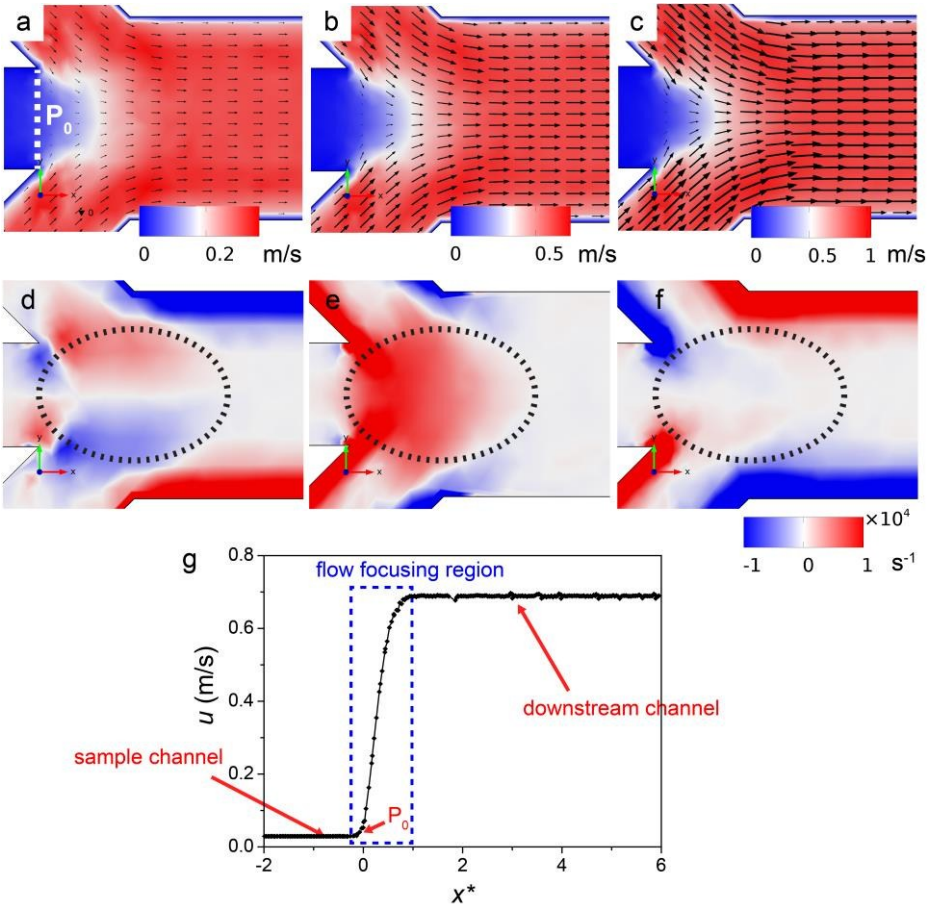

Fig 2 Numerical simulations of (a - c) velocity magnitude and (d - f) components of the deformation tensor in the absence of droplets on the *xy* plane (at half *z*) of the sheath flow focusing region. From (a) to (c), the central channel velocity v_d = 0.02 m/s; the sheath flow velocities v_s = 0.23 m/s (*Ca* = 0.006), 0.46 m/s (*Ca* = 0.012), and 0.69 m/s (*Ca* = 0.018), respectively. (d) Shear strain rate ($\partial u/\partial y + \partial v/\partial x$), (e) elongational strain rate ($|\partial u/\partial x| + |\partial v/\partial y|$) and (f) vorticity ($\partial v/\partial x - \partial u/\partial y$) at the flow condition of (b). (g) Plot of axial velocity *u* in (b) along the centre line of the microchannel. x^* is the axial coordinate normalised by the width of the channel *w*, *i.e.* $x^* = x/w$. P_0 marks the entrance of the sample flow (*or* droplets) to the sheath flow focusing region and wider channel, and set x^* (P_0) = 0. *u* and *v* are the axial and transverse velocity components. The inlet flow velocities were selected in accordance with the experimental studies reported herein. Dashed ellipses in (d -f) highlight the maximum deformation region. Downstream of the sheath flow focusing region a typical laminar channel flow is established, not shown here.

The microfluidic channel was placed on an inverted microscope (Olympus IX71, Olympus Optical Co. Ltd, Tokyo, Japan) and images and videos were captured by a high-speed CMOS camera (Phantom v7.3, Vision Research, USA) at a frame rate of approximately 20 kHz. All fluids were delivered to the microchannel by syringe pumps at flow rates (PHD 2000 Infusion Pump, Harvard Apparatus, USA) ranging from 200 to 15,000 µl/hr. The acquired images were processed using the open source software ImageJ™ in order to quantify deformation. W/o/w double emulsions were formed by sequentially injecting aqueous, oil and aqueous phases from inlets 1, 2, 3; w/o single droplets were formed by blocking inlet 1. Fluorinated EA-surfactants (RainDance Technologies, USA) were added at 0.5 wt% in the oil phase throughout the experiments. A series of fluorinated oils were used, including FC3283, FC40, FC70 (3M, USA), with corresponding oil phase dynamic viscosities of 1.4, 4.1 and 24 mPa·s, respectively. Various concentrations of sodium dodecyl sulphate (SDS) (L3771, Sigma, UK) and Tween 80 (P1754, Sigma, UK) were tested at the inner aqueous phase, DIW, while maintaining the outer aqueous phase being 0.5 wt% SDS in DIW. 10 wt% and 20 wt% Polyethylene glycol (M_W = 2000) (84797, Sigma, UK) were added to the inner aqueous phase in some cases to increase the core viscosity from 0.89 to 2.27 and 4.16 mPa·s. The inner-to-outer viscosity ratio λ_i varies from 0.037 to 3.0. (Table 1)

Journal Name

ARTICLE

Table 1 Physical parameters of the liquid-liquid systems used in this study (25 °C).[46-51]

μ and γ are the viscosity and surface tension of inner core *(i)* and outer oil *(o)* phases; λ and Γ are the viscosity ratio and surface tension ratio of inner-to-outer *(i)* and outer-to-sheath *(o)* phases, respectively.

	Fluids*		μ_i (mPa·s)	μ_o(mPa·s)	λ_i	λ_o
	Inner (*i*)**	Outer (*o*)***				
Viscosity effect	H_2O	FC3283	0.89	1.4	0.64	1.6
		FC40		4.1	0.22	4.6
		FC70		24	0.037	27
	10 wt% PEG in H_2O	FC3283	2.27	1.4	1.6	1.6
	20 wt% PEG in H_2O		4.16		3.0	
	Fluids		γ_i (mN/m)	γ_o (mN/m)	Γ_i	Γ_o
	Inner (*i*)	Outer (*o*)				
Surface tension effect	H_2O	0.5 wt% EA-surfactant in FC3283	72	9.2 ± 0.7	7.8	0.25
	0.5 wt% SDS in H_2O		37		4.0	
	2.0 wt% SDS in H_2O		34		3.7	
	0.25 wt% Tween 80 in H_2O		39		4.2	
	2.0 wt% Tween 80 in H_2O		38		4.1	

* The sheath fluid is kept as 0.5 wt% SDS in H_2O throughout the study; ** Inner phase is loaded with 0.5 wt% SDS; *** Outer phase is loaded with 0.5 wt% EA-surfactant.

The surface tension of surfactant-loaded fluorinated oil FC3283 was measured using the pendant droplet method,[45] which is an established technique. Measurements were performed at room temperature on a FTA1000 B Class contact angle instrument (First Ten Ångstroms, USA) equipped with a camera for video recording. The inner-to-outer surface tension ratio Γ_i ranges from 3.7 to 7.8, as shown in Table 1.

The sheath flow focusing region in Fig 1a is shown in more detail in Fig 1b; the sheath fluid enters the main channel flow from both sides at a 45° angle. Droplets decelerate and start deforming as they emerge from the main sample channel, adopting initially a pointed shape and then an elongated one as they encounter the sheath flow focusing junction, *i.e.* the region where the three inlet streams merge (see SI videos). Deformed double emulsions remain aligned with the channel centreline and gradually recover their initial morphologies further downstream. From conservation of mass the velocity in the wide channel is $v_{total} = v_s + v_c/2$ where v_c and v_s are the average velocities in the droplet formation channel and sheath flow channels respectively. The capillary number is hence defined as $Ca = \mu_s \cdot v_{total}/\gamma_s$, where μ_s and γ_s are the viscosity and surface tension of the sheath phase, respectively. The Reynolds number, $Re = \rho_s \cdot v_{total} \cdot D_H/\mu_s$, in this study varied from 12 to 35 for sheath flow rates of 0.23 to 0.69 m/s, where ρ_s and D_H are the density and the hydraulic diameter of the sheath fluid, respectively.

The two dimensional laminar flow in the sheath flow focusing microchannel geometry was simulated using Comsol Multiphysics® in order to obtain the distribution of velocity and hydrodynamic strain rates. Simulations were carried out in the absence of the compound droplet and with water as working fluid for all three streams. Fig 2 shows the predicted velocity flow field (in vector and contour forms) and the distribution of the strain and vorticity components of the deformation tensor in the sheath flow focusing region. The central channel velocity is kept at 0.02 m/s and sheath flow rates vary from 0.23 m/s (Ca = 0.006, Fig 2a), 0.46 m/s (Ca = 0.012, Fig 2b) and 0.69 m/s (Ca = 0.018, Fig 2c), to match the velocities employed in the experiment. Vector plots show a low velocity stream ensuing from the sample channel and merging with the faster flowing sheathing streams forcing the droplets to squeeze through and transiently deform. The ratio between the flow rates of the incoming sample and sheath streams determines the strain of deformation, *i.e.* the degree of shear or extensional strain. The velocity gradients at the sheath flow focusing region increase proportionally with increasing sheath flow velocities. Flow recovers further downstream to adopt the typical laminar velocity profile for rectangular channels. Figs 2d – 2f show the strain rate and vorticity distributions at the sheath flow focusing region for v_d = 0.02 m/s, and v_s = 0.46 m/s respectively: shear strain rate ($\partial u/\partial y + \partial v/\partial x$) (Fig 2d), elongational strain rate ($|\partial u/\partial x| + |\partial v/\partial y|$) (Fig 2e), and vorticity ($\partial v/\partial x - \partial u/\partial y$) (Fig 2f), where u and v are the axial and transverse velocity components. It should be noted that the gradients du/dx and dv/dy are equal in magnitude and of opposite sign (as expected by the incompressibility condition for a 2D flow). Hence the

magnitude of the gradients is used for the elongational strain rate calculation. Figs 2d - 2f demonstrate the predominantly extensional nature of the flow at the focusing region as evidenced by the distribution of elongational strain rate and the absence of rotation (near zero vorticity rates) in the central part of the channel. However, the shear component of the deformation tensor is not negligible as can be seen by Fig 2d. Fig 2g shows the axial velocity profile along the channel centreline. It can clearly be seen that there is a region of about one channel width w in which the axial velocity rises steeply and in a linear manner until it attains a constant value, *i.e.* the maximum velocity for the fully developed microchannel flow further downstream. This is the region where droplet deformation takes place. The linear increase in velocity with axial distance implies a constant extension rate du/dx similar to extensional flow in a hyperbolic contraction.

It should be noted that previous studies have employed either pure extensional or shear flows to study deformation of droplets. Four mill devices[24] or hyperbolic contractions[36] have been employed to generate such model flows in order to decouple the effects of shear and extensional deformation. In the present study droplets deform in a transient manner as they encounter the sheath flows which, for the given flow rate ratio, generate a region of extensional flow along the centreline. It should be noted that the wide aspect ratio of the channel employed (nearly 1/10) implies that shear stresses will be significantly higher in the *yz* plane and will have an effect on the droplet deformation in that plane which cannot be visualized in the present study. However, as the droplet is always confined by the top and bottom channel walls, monitoring its shape in the *yz* plane is not meaningful; the deformation in the *xy* plane thus provides a better indication of the sheath flow focusing effect in practical applications such as FACS. The small channel height affects the double emulsion (core) morphology: droplets are flattened and are subjected to friction from the top and bottom channel surfaces that affect the droplet mobility and possibly deformation. By tracking the flowing droplets it was found that in the narrow channel, *i.e.* upstream of the sheath flow focusing region, the droplet velocity v_d is generally close to that of the continuous phase v_c, except in the vicinity of the focusing point where the droplet decelerates; however, in the wide channel and after passing through the sheath flow focusing region, v_d is smaller than the continuous phase velocity v_{total} due to wall friction. (Fig S1) In addition, the double emulsion (core) morphology does not fully recover after deformation as discussed in the following section.

Results and Discussion

a. Deformation of single droplets vs inner cores of double emulsions

Deformation, of both droplets and inner cores of double emulsions, is typically quantified using the dimensionless number D, defined as

$$D = \frac{a-b}{a+b}$$

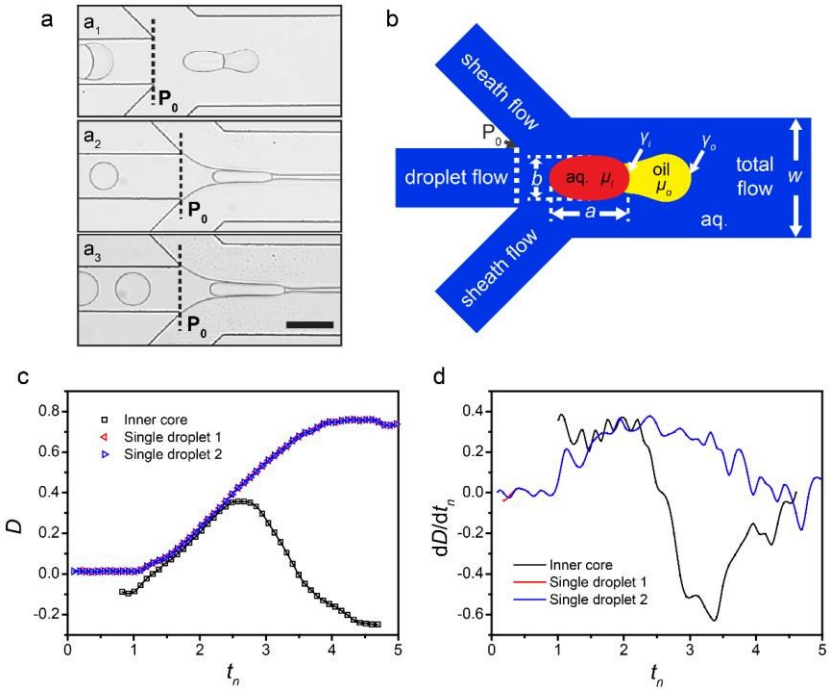

Fig 3. Comparison of single droplets and the inner core of a double emulsion deformation. (a) Snapshot of (a_1) an inner core (0.13 nl) and (a_2, a_3) two single droplets (0.11 nl and 0.16 nl) being deformed by the sheath flow focusing effect. (b) Schematic of the double emulsion showing major and minor axes a and b and viscosity ratio notation. (c) Deformation as a function of time of the inner core and two different sized single droplets flowing through the sheath focusing junction. t_n is the normalised time scale, with $t_n = t \cdot v_{total}/w$. (d) Rate of deformation dD/dt_n for the droplets in (c). v_s = 0.46 m/s and v_d = 0.02 m/s (Ca = 0.012), respectively. The aqueous phases (single droplet, core, outer and sheath fluids) are 0.5 wt% SDS in DIW, and the oil shell phase is FC3283 with EA surfactant. Inner-to-outer viscosity ratio λ_i = 0.64, and surface tension ratio Γ_i = 4.0.

Journal Name

ARTICLE

where a is the droplet axial dimension and b is the transverse dimension.[17,21,36] The deformation index D is used for low deformations whereas the ratio a/b is preferred for larger deformations. In this study both indices were estimated and resulted in similar trends; hence results will be presented in terms of the widely used index D in this study. Unlike stationary single droplets or droplets moving at low Ca in confined microchannels that deform from an initially spherical shape with a value of $D = 0$, the inner cores of moving double emulsions in this study exhibit a slightly different morphology prior to sheath flow focusing. The double emulsions studied here are partially engulfed with the inner core pushed to the rear of the shell and slightly elongated in the transverse direction. Thus D is negative prior to sheath flow deformation (see SI videos and Fig 3a). When passing through the sheath flow focusing region, the inner cores (as well as the outer shell) elongate with time, increasing in length a and decreasing in width b (Fig 3b) and reaching a maximum deformation value, D_{max}, at the sheath focusing site (indicated by the waist thinning of the double droplet in SI videos), after which the deformed core and shell gradually recover their shape. As the outer shell engulfs the inner core, and acts as the intermediate phase between the inner core and the sheath fluid, the outer shell generally deforms more, at least in certain regions, than the inner core in agreement with numerical studies for fully engulfed droplets.[23] However, in flow cytometry applications the inner core deformation is of particular importance as it determines the microenvironment that the encapsulated cells for screening are exposed to. For this reason, this study focuses mainly on the inner rather than outer droplet deformation. It should be noted that throughout the double emulsion deformation study, the volume ratio of inner core to outer shell, k, is maintained at 1, by controlling the delivery of both fluid phases at equal rates, unless noted otherwise.

Figure 3a shows selected snapshots of a double emulsion and two different sized single droplets at their maximum deformation. As shown in the figure, the aqueous single droplets are carried by the middle oil phase and are confined between the two aqueous converging sheath streams flowing with the same high velocity into the central channel and forcing the droplets to elongate. As the core fluid is oil in this case a thread is formed along the channel centreline. Fig 3b defines the dimensions a and b used to quantify the deformation index of the double emulsions. Fig 3c shows the deformation as a function of time of the single droplets and the inner core in Fig 3a; the aqueous inner core (0.13 nl) is the intermediate of the two single droplets (0.11 nl and 0.16 nl) in size. As shown in Fig 3c, the deformation D of the two single droplets follows exactly the same pattern; the single droplets reach a maximum deformation value of 0.7 and remain deformed for the remaining length of the straight channel downstream of the flow focusing junction (not shown in figure). On the contrary, the deformation index of the inner core of the double emulsion attains much lower values with D_{max} reduced to half the value of single droplets (D_{max} = 0.3). The deformation time is normalised with the characteristic time scale of the flow given by w/v_{total} where w and v_{total} are the channel width and total velocity respectively (*i.e.* $t_n = t \cdot v_{total}/w$), and v_{total}/w represents the average shear rate in the wide channel. The droplet deformation starts at approximately t_n = 1.0; the maximum deformation is reached after an elongation phase occurring at a rate similar to that of the single droplet at t_n = 2.5 followed by a rapid recovery stage in which the double emulsions regain their pre-deformation morphology as shown in Fig 3. As the flow rate of the single droplets and the double emulsion is increased approximately 20-fold after merging with the sheath flow, the equilibrium morphology is reached after t_n = 4.5, corresponding to a distance of 1 mm downstream of P_0, that marks the entrance to the wide downstream channel where all streams merge. At this point equivalent single droplets have attained their maximum deformation and have not started recovering their shape yet. Fig 3d shows the rate of deformation (dD/dt_n) for the droplets shown in Fig 3c, obtained by forward differencing of D in time. The inner core shows lower elongation rate but higher recovery rate compared to single droplets. The inner core shape recovery seems rapid whereas the single droplets appear to have reached steady-state deformation within the observation time as indicated by the fluctuating around zero values of dD/dt_n. Data is not shown further downstream as the observed droplet/core morphology fluctuated as the channel outlet is approached. Interestingly, the recovered morphology of double droplets is not exactly the same as pre-deformation, possibly due to the changes in the flow rate, or Ca, the degree of confinement, C, and friction by the top and bottom channel surfaces. Variation in the wetting behaviour (or contact angles) between core and shell phases might also have an effect on double emulsion deformation.

b. Effect of viscosity ratio

The viscosity plays a significant role in droplet and double emulsion deformation, as shear stresses are viscosity dependent for a given velocity gradient. As the oil phase acts as a shell or separating layer between the inner core and the sheath flow focusing fluid, we deduce that increasing the viscosity of the oil phase reduces the core deformation. In Fig 4, by changing the oil phase from FC3283 to FC40 and then FC70, with 0.5 wt% EA-surfactant, the shell viscosity progressively increases (Table 1) resulting in core-to-shell viscosity ratios, λ_i, decreasing from 0.64 to 0.22 and 0.04, and outer-to-sheath

viscosity ratio, λ_o, increasing from 1.6 to 4.6 and 27, respectively, for cores made of 0.5 wt% SDS in DIW; by adding 10 wt% or 20 wt% PEG into the core phase, while retaining the shell being FC3283 with EA surfactant, λ_i accordingly increases from 0.64 to 1.6 and 3.0. Hence, (1) decreasing core-shell viscosity ratio λ_i by increasing the viscosity of the oil phase, or (2) increasing λ_i by increasing the viscosity of the core phase likewise affects the transient core deformation behaviour; peak deformation, D_{max}, is reached earlier and decreases in value; shape recovery also starts earlier (Fig 4c and 4e). It should be noted however that by changing the oil phase the outer viscosity ratio changes, which affects the deformation of the outer droplet. Fig 4d shows the rate of deformation against t_n. Droplets exhibiting large deformation in Fig 4c show high rates of recovery. The highest deformation rate occurs at $t_n = 4 \sim 5$, which corresponds to the core recovery regions. The cores with the lowest and highest viscosity ratio (blue and purple curves in Fig 4c) show very low rates of deformation as they deform relatively less. As surfactants were loaded at low concentrations in either oil or aqueous phases, we assume that fluid viscosities were not altered throughout the study. Fig 4e shows a non-monotonic dependence of core deformation on inner viscosity ratio in which maximum deformation increases with core-to-shell viscosity ratio λ_i for values less than around 1 and decreases for ratios exceeding this value. However, it should be noted that the outer viscosity ratio λ_o is kept constant only in the high λ_i ratio cases (*i.e.* the decreasing deformation part) and hence an effect of λ_o should be expected for λ_i smaller than 1. Such non-monotonic behaviour has previously been reported for single droplet deformation in a microfluidic junction[52] in which three deformation regimes were observed for low, moderate and high viscosity ratios: deformation was independent of viscosity ratio for values less than 0.01, increased for values up to 1 or 2 and then decreased for high viscosity ratios above 10. This was attributed to the combined effects of the stresses by both surrounding and inner fluids acting on the interface and the interfacial relaxation time of the droplet which is viscosity ratio dependent. When the viscosity ratio increases from small values up to around 1 the interfacial relaxation time of the droplet increases moderately allowing sufficient time for the droplet to deform under the action of the inner and outer fluid forces; hence droplet deformation increases with viscosity ratio. On the contrary, in more viscous droplets deformation depends on inner fluid stresses only; such droplets react slower to the flow focusing effect and hence deformation as well as relaxation are slower. The role of viscosity in double emulsion droplets is more complex and not systematically investigated. Qu and Wang[25] studied numerically the effect of viscosity ratio for concentric droplets and found an increase in core and shell deformation with outer viscosity for moderate values only (10^{-2} to 10) and a decrease with inner viscosity ratio for low values between 0.01 and 1. These trends are similar to those observed in the present study for inner core deformation. (Fig 4e) However, it should be borne in mind that viscosity ratios are defined with respect to continuous phase in their study and hence they can be independently controlled.

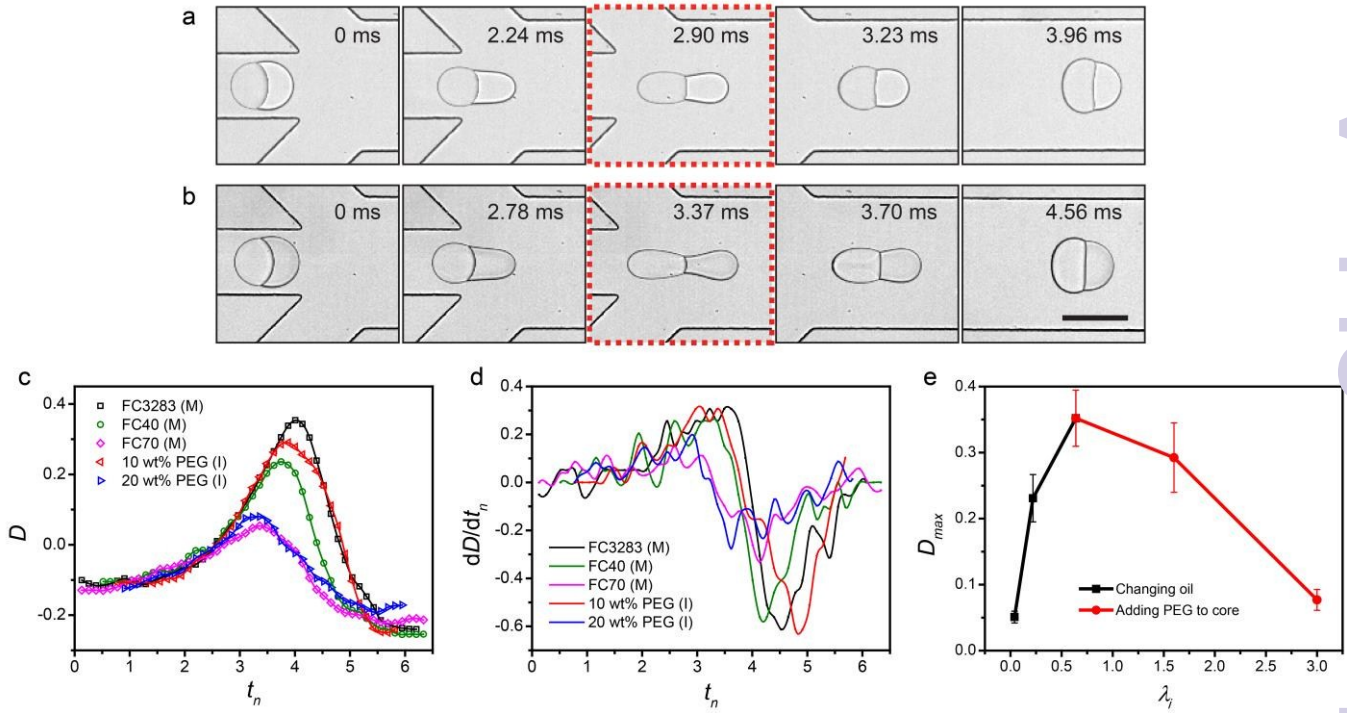

Fig 4 Selected snapshot sequences of deforming double emulsions for (a) FC40, and (b) FC3283, both loaded with EA-surfactant as oil phase and 0.5 wt% SDS in DIW as the inner core phase (λ_i(a) = 0.22, λ_i(b) = 0.64). (c) Deformation as a function of t_n of inner cores of different viscosity ratios: 0.5 wt% SDS in DIW (core, I) in FC3283, FC40, or FC70, loaded with 0.5 wt% EA surfactant (shell, M), corresponding to λ_i = 0.64, 0.22 and 0.04, respectively; and 10 wt% PEG or 20 wt% PEG in DIW (core, I) in FC3283, loaded with EA surfactant (shell, M), corresponding to λ_i = 1.6 and 3.0, respectively. (d) Rate of deformation dD/dt_n for the cores in (c). (e) Maximum core deformation, D_{max}, as a function of λ_i in (c). The black and red curves represent the core being 0.5 wt% SDS in DIW but changing the oil, or the shell being FC3283 with EA-surfactant but adding PEG to core, respectively. v_s = 0.46 m/s and v_d = 0.02 m/s (Ca = 0.012), respectively. Red dash frames in sub figures (a, b) indicate the maximum deformation of the double emulsions.

Journal Name

ARTICLE

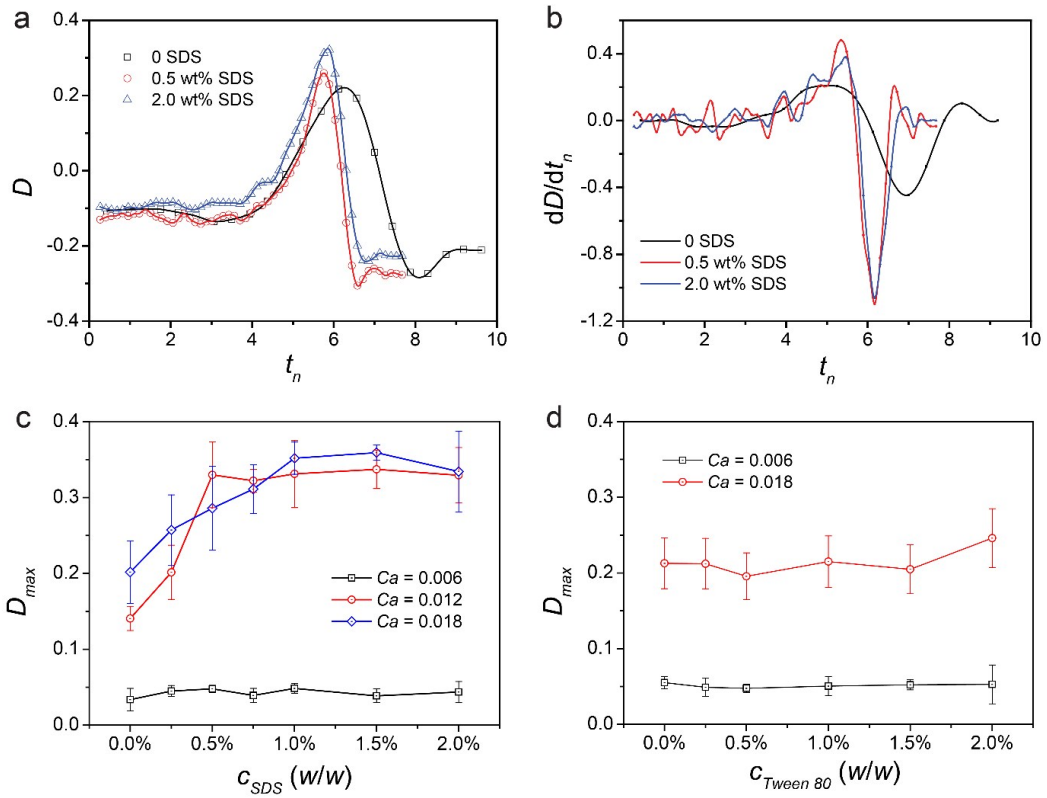

Fig 5 Effect of surfactant on inner core deformation. (a) Deformation as a function of time for inner cores loaded with 0, 0.5 wt% and 2.0 wt% SDS, respectively. v_s = 0.69 m/s (*Ca* = 0.018). (b) Rate of deformation of droplets in (a). (c) Variation of maximum core deformation, D_{max}, with SDS surfactant concentrations in the core phase and v_s = 0.23, 0.46, and 0.69 m/s (*Ca* = 0.006, 0.012, and 0.018). (d) Variation of D_{max} with Tween 80 surfactant concentrations in the core phase and v_s = 0.23 and 0.69 m/s (*Ca* = 0.006 and 0.018). The oil and other aqueous fluids are FC3283 with EA-surfactant, and 0.5 wt% SDS in DIW. λ_i = 0.64 and v_d = 0.02 m/s.

c. Role of surfactants

Surfactant molecules adsorbed to the oil-water interface reduce the interfacial tension; under elongation and shearing strain, surfactant molecules migrate and a concentration gradient appears along the interface. Restricted by their lateral mobility, surfactant molecules concentrate more near a pole on a droplet, hence decreasing the interfacial tension locally and inducing a 'softer' interface and enhanced deformation.[53] Numerous studies have reported on the role of surfactants on droplet deformation by mainly affecting the external shear stresses;[53-55] less work has been published on the surfactant effects on compound droplet deformation under shear flow,[25,26] and there has been no reported study on surfactant-dependent deformation of double emulsions under sheath flow focusing.

Figure 5a compares the transient core deformation of double emulsions composed of cores with 0, 0.5, and 2.0 wt% SDS in DIW respectively. The middle oil phase and the other aqueous phases (the outer phase and the sheath fluid) are 0.5 wt% EA surfactant in FC3283 and 0.5 wt% SDS in DIW, respectively. Cores without added surfactant (0 SDS) exhibit lower deformability (D_{max}) and their shape recovery is more prolonged, demonstrating that non-surfactant laden emulsions have less deformable interfaces. Core deformation D varies little with surfactant concentration as indicated by the deformation transients for 0.5 wt% and 2.0 wt% SDS. Fig 5b shows similar deformation rates for the two surfactant concentration cases; the maximum rate dD/dt_n occurs at the recovery regime which is rapid (t_n less than 1, *i.e.* half the elongation phase). This weak dependence could be partly attributed to the small reduction of interfacial tension achieved at concentration levels exceeding a critical value, and partly to the limited lateral mobility of the surfactant molecules. A kinetics study showed that surfactant molecules buildup at the interface of a w/o droplet on a time scale varying from milli-

seconds to seconds,[56] indicating that surfactant migration in droplet formation and deformation in microfluidics is time-dependent.

The influence of SDS concentration on maximum core deformation D_{max} is plotted in Fig 5c for three sheath flow velocities. At the lowest sheath flow velocity (0.23 m/s, Ca = 0.006), the velocity gradient between sheath flow and central channel flow is reduced, resulting in lower shear stresses; thus D_{max} is significantly lower than that at higher sheath flow rates (0.46 m/s, Ca = 0.012 and 0.69 m/s, Ca = 0.018). However, the D_{max} does not vary significantly when the sheath velocity increases from 0.46 m/s (Ca = 0.012) to 0.69 m/s (Ca = 0.018), especially after exceeding 0.5 wt% SDS concentration.

The surface tension of stationary SDS aqueous solutions remains constant for concentrations 0.2 wt% and above;[47,50] however, the critical concentration might be different in microfluidic droplets as the time scale from double emulsion formation to sheath flow focusing is not sufficient for surfactant molecules to migrate and reach equilibrium on the interface.[56-58] Hence the critical SDS concentration shifts from 0.2 wt%, to a higher value, *i.e.* 0.5 wt% in the present study.

Moreover the present study indicates that the surfactant dependence of double emulsion deformation is molecule-related: the maximum core deformation, D_{max}, does not depend significantly on surfactant concentration when inner cores are loaded with 0 to 2.0 wt% Tween 80, as shown in Fig 5d. As the molecule size is a critical factor on the lateral mobility of surfactant molecules, it is reasonable to conclude that the large molecule surfactant Tween 80 (M_W = 1310 g/mol) has lower mobility than the small molecule SDS (M_W = 288 g/mol) on the w/o interface,[48,59] which might result in the negligible influence of the Tween 80 concentration on core deformation, despite the similar values of surface tension ratios. (Table 1)

d. Effect of droplet velocity ratio and inner core size

So far the double emulsion core deformation has been found to be affected more significantly by the viscosity of either the shell oil or inner aqueous phase, than the surfactant concentration in the inner core phase. However, the deformation of the double emulsions studied here is caused primarily by the extensional nature of the flow generated at the sheath flow focusing region due to the fast sheath flows in relation to the central channel flow. Therefore it is reasonable to expect a relationship between core deformation, sample channel (double emulsion) flow velocity, v_d, and sheath flow velocity, v_s. The droplet velocity ratio β is defined as $\beta = v_d/v_{total}$. At small β, the sheath flows merge at a high speed creating a highly extensional flow at the focusing point that results in increased droplet deformation, as shown in Fig 6a. As β increases the maximum core deformation D_{max} reduces to levels comparable to those pre-deformation, *i.e.* the cores hardly deform if β exceeds 0.1. Hence to maintain the same level of D_{max} at different sample velocities, v_d, the sheath flow rates should be varied accordingly, to maintain β within a certain range.

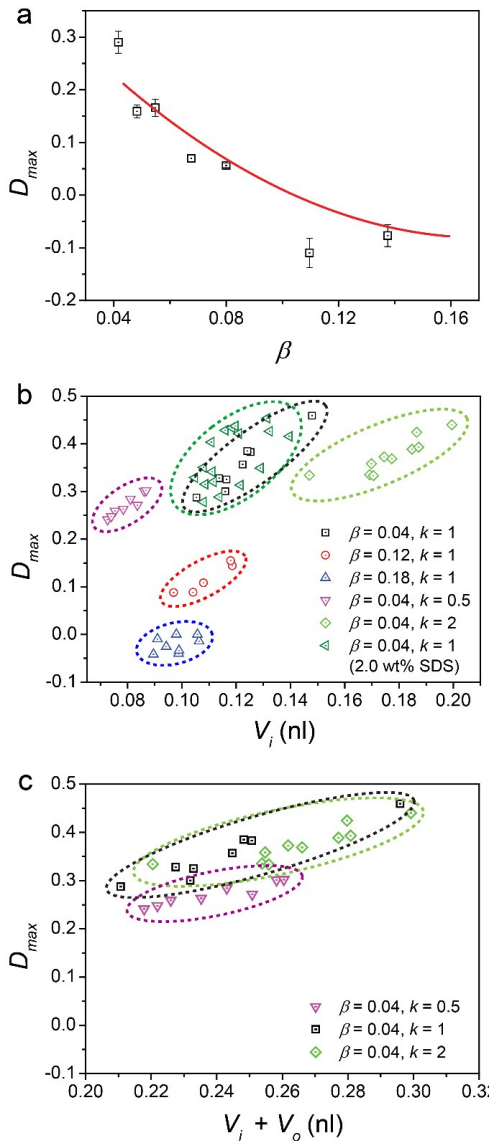

Fig 6 Effects of droplet velocity ratio β and core-shell size ratio k on inner core deformation. (a) D_{max} dependence on β. (b) Dependence of D_{max} on inner core volume V_i, at varying k, β, and SDS concentrations in cores. (c) Dependence of D_{max} on double emulsion volume ($V_i + V_o$) for different k. All populations of cores are loaded with 0.5 wt% SDS in DIW, except for the labelled population, with 2.0 wt% SDS. The oil phase is FC3283 with EA surfactant. v_s = 0.69 m/s and λ_i = 0.64.

It has been reported that the degree of confinement affects droplet deformation: generally at a given Ca, droplet deformation grows with the degree of confinement C, defined as the droplet diameter over the channel width, when $C < 1$.[36] In the present study, double emulsions are visualised as 2D ellipsoids with their minor axis always smaller than the channel width, and hence $C < 1$. For double emulsions, there are two factors affecting the degree of confinement: core volume, V_i, and core-to-shell size ratio, k. The core volume was estimated by measuring the area of the imaged cores and multiplying by the channel depth; this gives an approximate volume and is justified by the wide aspect ratio of the channel which 'flattens' the droplets. The size ratio was controlled by tuning the flow rate ratio of the inner aqueous to middle oil phases. The core

volume is a measure of confinement for a given size ratio k ($C \propto V_i^{0.5}$); as the core volume increases D_{max} increases with V_i for a given β and k, as shown in Fig 6b. The deformation data for β = 0.04, k = 0.5, 1 and 2 in Fig 6b varies significantly in core volume, V_i, but the maximum deformation values D_{max} do not differ significantly, especially those for core–shell ratios k of 1 and 2. However, when the entire double emulsion volume (V_i + V_o) is considered, the deformation data D_{max} for various size ratios at a given velocity ratio β collapse (Fig 6c), indicating that D_{max} relates not only to core volume but also the shell volume. Thus to consider the degree of confinement, both V_i and V_o should be considered. However, further work is required to establish the exact relationship, which is beyond the scope of this study.

The overlapping data for the two populations of β = 0.04, k = 1 with 0.5 wt% and 2.0 wt% SDS verify the conclusion from Fig 5, that SDS concentration has no significant effect on core deformation above a critical value. The deformation data for β = 0.04, 0.12, and 0.18, k = 1 in Fig 6b is also in good agreement with the trend of D_{max} against β in Fig 6a.

Conclusions

The deformation of partially engulfed double emulsions under sheath flow focusing conditions similar to those encountered in flow cytometry were studied. It was found that w/o single droplets deform more than w/o/w double emulsions under certain aqueous sheath flow focusing: the deformed single droplets cannot recover their non-deformed morphologies as they remain in confinement longer, whereas double emulsions recover their non-deformed morphology rapidly downstream of the sheath focusing point. Viscosity, core and shell volume and flow rate significantly affect core deformation: increasing either core or shell viscosity decreases core deformation, while increasing sheath flow rate and core size increases core deformation. The shell size does affect core deformation, and hence both core volume and core-to-shell size ratio (or double emulsion volume) should be considered in the prediction of core deformation. The dependence of core deformation on surfactant is less pronounced and surfactant type related; low molecular weight surfactants like SDS enhance core deformation for concentrations up to a critical value; core deformation becomes independent of surfactant concentration when this critical value is exceeded. Moreover, high molecular weight surfactants like Tween 80 do not significantly affect core deformation.

The study provides useful guidelines for the design of w/o/w systems for flow cytometry: to reduce deformation of aqueous cores of w/o/w double emulsions passing through the sheath flow focusing, such as applying double emulsion compartmentalisation in flow cytometry, it is beneficial to load less surfactant in the core phase, adopt smaller double emulsions, increase the viscosity of the core and/or the shell phases and increase sample flowrate in relation to sheath flow. However, at a given velocity gradient, higher viscosity induces increased stresses; thus to maintain the low stress levels in aqueous cores, where the biological samples would be compartmentalised, it is best to increase shell viscosity to obtain lower deformation and viscous stresses. Higher viscosity also results in higher levels of hydrodynamic resistance. Increasing sample flow rate in relation to sheath flow will result in smaller velocity gradients between the streams and hence lower deformation stresses. Moreover, surfactant concentration is correlated with emulsion stability, and must be loaded above certain levels, depending on the application. Thus all these factors must be carefully considered in designing compartmentalisation systems. Although the present study was designed with the flow cytometry application in mind, it can serve as a validation tool for the numerous numerical studies on compound droplet deformation. It also demonstrates that sheath flow focusing might serve as an alternative platform for flow induced deformation studies of objects such as vesicles and capsules.

References

1 A. B. Theberge, F. Courtois, Y. Schaerli, M. Fischlechner, C. Abell, F. Hollfelder, and W. T. S. Huck, *Angew. Chemie Int. Ed.*, 2010, **49**, 5846–5868.
2 S.-Y. Teh, R. Lin, L.-H. Hung, and A. P. Lee, *Lab Chip*, 2008, **8**, 198–220.
3 H. N. Joensson and H. Andersson-Svahn, *Angew. Chem. Int. Ed.*, 2012, **51**, 12176–12192.
4 E. Z. Macosko, A. Basu, R. Satija, J. Nemesh, K. Shekhar, M. Goldman, I. Tirosh, A. R. Bialas, N. Kamitaki, E. M. Martersteck, J. J. Trombetta, D. A. Weitz, J. R. Sanes, A. K. Shalek, A. Regev, and S. A. McCarroll, *Cell*, 2015, **161**, 1202–1214.
5 A. M. Klein, L. Mazutis, I. Akartuna, N. Tallapragada, A. Veres, V. Li, L. Peshkin, D. A. Weitz, and M. W. Kirschner, *Cell*, 2015, **161**, 1187–1201.
6 C. Martino, S.-H. Kim, L. Horsfall, A. Abbaspourrad, S. J. Rosser, J. Cooper, and D. A. Weitz, *Angew. Chem. Int. Ed Engl.*, 2012, **51**, 6416–6420.
7 S.-H. Kim, H. C. Shum, J. W. Kim, J.-C. Cho, and D. A. Weitz, *J. Am. Chem. Soc.*, 2011, **133**, 15165–15171.
8 F. Meng, G. H. M. Engbers, and J. Feijen, *J. Control. Release*, 2005, **101**, 187–198.
9 J. Thiele, A. R. Abate, H. C. Shum, S. Bachtler, S. Förster, and D. A. Weitz, *Small*, 2010, **6**, 1723–1727.
10 W. Wang, M.-J. Zhang, R. Xie, X.-J. Ju, C. Yang, C.-L. Mou, D. A. Weitz, and L.-Y. Chu, *Angew. Chem. Int. Ed.*, 2013, **52**, 8084–8087.
11 S. Ma, J. Thiele, X. Liu, Y. Bai, C. Abell, and W. T. S. Huck, *Small*, 2012, 2356–2360.
12 D. J. McClements, *Curr. Opin. Colloid Interface Sci.*, 2012, **17**, 235–245.
13 M. Marguet, L. Edembe, and S. Lecommandoux, *Angew. Chemie*, 2012, **124**, 1199–1202.
14 J. Thiele, V. Chokkalingam, S. Ma, D. A. Wilson, and W. T. S. Huck, *Mater. Horizons*, 2014, **1**, 96–101.
15 S. Guido, *Curr. Opin. Colloid Interface Sci.*, 2011, **16**, 61–70.
16 S. Guido and V. Preziosi, *Adv. Colloid Interface Sci.*, 2010, **161**, 89–101.
17 C. Ulloa, A. Ahumada, and M. L. Cordero, *Phys. Rev. E*, 2014, **89**, 033004.
18 P. Dimitrakopoulos and S. Kuriakose, *Soft Matter*, 2015, **11**, 2782–2793.
19 A. Vananroye, P. J. Janssen, P. D. Anderson, P. Van Puyvelde, and P. Moldenaers, *Phys. Fluids*, 2008, **20**, 1–10.
20 A. Gupta and M. Sbragaglia, *Phys. Rev. E* 2014, **90**, 023305.

21 G. I. Taylor, *Proc. R. Soc. London, Ser. A*, 1934, **146**, 501–523.
22 R. E. Johnson and S. S. Sadhal, *Annu. Rev. Fluid Mech.*, 1985, **17**, 298–320.
23 J. Guzowski, P. M. Korczyk, S. Jakiela, and P. Garstecki, *Soft Matter*, 2012, **8**, 7269.
24 H. A. Stone and L. G. Leal, *J. Fluid Mech.*, 1990, **211**, 123–156.
25 X. Qu and Y. Wang, *Phys. Fluids*, 2012, **24**, 123302.
26 H. Hua, J. Shin, and J. Kim, *Int. J. Heat Fluid Flow*, 2014, **50**, 63–71.
27 C. Zhou, P. Yue, and J. J. Feng, *Int. J. Multiph. Flow*, 2008, **34**, 102–109.
28 J. Tao, X. Song, J. Liu, and J. Wang, *Chem. Eng. Sci.*, 2013, **97**, 328–336.
29 L. B. Leverett, J. D. Hellums, C. P. Alfrey, and E. C. Lynch, *Biophys. J.*, 1972, **12**, 257–273.
30 M. A. Garcia-Briones and J. J. Chalmers, *Biotechnol. Bioeng.*, 1994, **44**, 1089–1098.
31 N. Gregoriades, J. Clay, N. Ma, K. Koelling, J. J. Chalmers, *Biotechnol. Bioeng.*, 2000, **69**, 171–182.
32 N. J. Douville, P. Zamankhan, Y.-C. Tung, R. Li, B. L. Vaughan, C.-F. Tai, J. White, P. J. Christensen, J. B. Grotberg, and S. Takayama, *Lab Chip*, 2011, **11**, 609–619.
33 J. Yan, W. A. C. Bauer, M. Fischlechner, F. Hollfelder, C. F. Kaminski, and W. T. S. Huck, *Micromachines*, 2013, **4**, 402–413.
34 S. Ma, J. M. Sherwood, W. T. S. Huck, and S. Balabani, *Lab Chip*, 2015, **15**, 2327–2334.
35 M. Mollet, R. Godoy-Silva, C. Berdugo, and J. J. Chalmers, *Biotechnol. Bioeng.*, 2008, **100**, 260–272.
36 M. K. Mulligan and J. P. Rothstein, *Phys. Fluids*, 2011, **23**, 022004.
37 C. Chung, J. M. Kim, M. A. Hulsen, K. H. Ahn, and S. J. Lee, *Chem. Eng. Sci.*, 2009, **64**, 4515–4524.
38 M. K. Mulligan and J. P. Rothstein, *Langmuir*, 2011, **27**, 9760–9768.
39 E. Lorenceau, A. S. Utada, D. R. Link, G. Cristobal, M. Joanicot, and D. A. Weitz, *Langmuir*, 2005, **21**, 9183–9186.
40 E. Q. Li, J. M. Zhang, and S. T. Thoroddsen, *J. Micromechanics Microengineering*, 2014, **24**, 015019.
41 W. A. C. Bauer, M. Fischlechner, C. Abell, and W. T. S. Huck, *Lab Chip*, 2010, **10**, 1814–1819.
42 Y. Xia and G. M. Whitesides, *Annu. Rev. Mater. Sci.*, 1998, **28**, 153–184.
43 S. Ma, J. M. Sherwood, W. T. S. Huck, S. Balabani, *Lab Chip*, 2014, **14**, 3611–3620.
44 MicroChem, http://www.microchem.com/Prod-SU82000.htm, (accessed June 2015).
45 X. Wang, A. Brandvik, and V. Alvarado, *Energy and Fuels*, 2010, **24**, 6359–6365.
46 T. Murugesan and M. Perumalsamy, *J. Chem. Eng. Data*, 2005, **50**, 1290–1293.
47 F. Hernainz and A. Caro, *Colloids Surf A: Physicochem. Eng. Asp.*, 2002, **196**, 19–24.
48 S. C. Kothekar, A. M. Ware, J. T. Waghmare, and S. A. Momin, *J. Dispers. Sci. Technol.*, 2007, **28**, 477–484.
49 A. J. Prosser and E. I. Franses, *Colloids Surf A: Physicochem. Eng. Asp.*, 2001, **178**, 1–40.
50 L. Zhang, S. Zhou, S. Wang, L. Wang, and J. Li, *J. Environ. Prot.*, 2013, **04**, 42–48.
51 3M™, http://www.mgchemicals.com/products/cleaners/3m-fluids/engineered-liquids/, (accessed June 2015).
52 H. A. Stone and L. G. Leal, *J. Fluid Mech.*, 1990, **220**, 161–186.
53 N. Boruah, P. Dimitrakopoulos, *J. Colloid Interface Sci.* 2015, **453**, 216–225.
54 K. Feigl, D. Megias-Alguacil, P. Fischer, and E. J. Windhab, *Chem. Eng. Sci.*, 2007, **62**, 3242–3258.
55 X. Li and C. Pozrikidis, *J. Fluid Mech.*, 1997, **341**, 165–194.
56 J.-C. C. Baret, F. Kleinschmidt, A. El Harrak, A. D. Griffiths, A. E. Harrak, and A. D. Griffiths, *Langmuir*, 2009, **25**, 6088–6093.
57 V. B. Fainerman, S. V. Lylyk, E. V. Aksenenko, N. M. Kovalchuk, V. I. Kovalchuk, J. T. Petkov, and R. Miller, *J. Colloid Interface Sci.*, 2012, **377**, 1–6.
58 M. R. de Saint Vincent, J. Petit, M. Aytouna, J. P. Delville, D. Bonn, and H. Kellay, *J. Fluid Mech.*, 2012, **692**, 499–510.
59 J. K. Ferri and K. J. Stebe, *Adv. Colloid Interface Sci.,* **2000**, 85, 61-97.